

RESEARCH ARTICLE SUMMARY

CLATHRIN ADAPTORS

HIV-1 Nef hijacks clathrin coats by stabilizing AP-1:Arf1 polygons

Qing-Tao Shen,* Xuefeng Ren,* Rui Zhang,* Il-Hyung Lee, James H. Hurley†

INTRODUCTION: Clathrin-coated vesicles mediate endocytosis and sorting from the trans-Golgi network (TGN) and endosomes to lysosomes. Adaptor protein (AP) complexes such as AP-1 connect membrane proteins to clathrin. AP-1 needs to be “unlocked” by activators in order to bind cargo and clathrin. The small guanine triphosphatase Arf1 unlocks AP-1 at the TGN by coupling AP-1:Arf1 dimerization to conformational changes. Major histocompatibility class I (MHC-I) proteins and the viral restriction factor tetherin are normally present on the cell surface. The viruses HIV-1, HIV-2, and simian immunodeficiency virus (SIV) use their Nef proteins to hijack clathrin and AP-1 and thus redirect MHC-I and tetherin to lysosomes.

RATIONALE: The down-regulatory functions of Nef are important for HIV-1 infectivity. Previous structural studies of Nef and AP complexes revealed that Nef only binds to unlocked APs. We sought to determine whether Nef could potentiate the physiological unlocking mechanisms in down-regulation of tetherin and

MHC-I. We used Förster resonance energy transfer (FRET) to determine the conformation of AP-1 complexes bound to Arf1, Nef, and cargo. To understand the mechanism by which Nef hijacks AP-1, we determined the structures of trimeric AP-1:Arf1:tetherin-Nef complexes by cryo-electron microscopy (cryo-EM) in active and inactive conformations. We predicted that the active AP-1:Arf1 trimer could form hexagonal lattices, which we visualized directly. To study the function of the hexagons, we reconstituted clathrin cage formation *in vitro* and showed that mutations in the lattice contacts blocked Arf1- and Nef-promoted cage formation.

RESULTS: In the presence of a tetherin-Nef fusion protein, AP-1:Arf1 complexes became trimeric. FRET analysis revealed that individual AP-1 complexes in the trimer were in the unlocked state. With the use of cryo-EM, we identified two kinds of trimers: closed and open. The closed trimer yielded a 7 Å reconstruction, which allowed docking of known atomic models of unlocked AP-1, Arf1, and Nef. The trimer is centered on a trimeric Arf1 interface. Although AP-1

was unlocked, the closed trimer hides the membrane binding sites and is thus inactive. The open trimer was more mobile, and the structure was resolved to 17 Å. The open trimer preserved the Arf1 trimeric interface while exposing membrane binding sites. Docking the open trimer with the known AP-1:Arf1 dimer yielded a hexagonal model that matched the dimensions of clathrin. The hexagons were visualized in

ON OUR WEB SITE

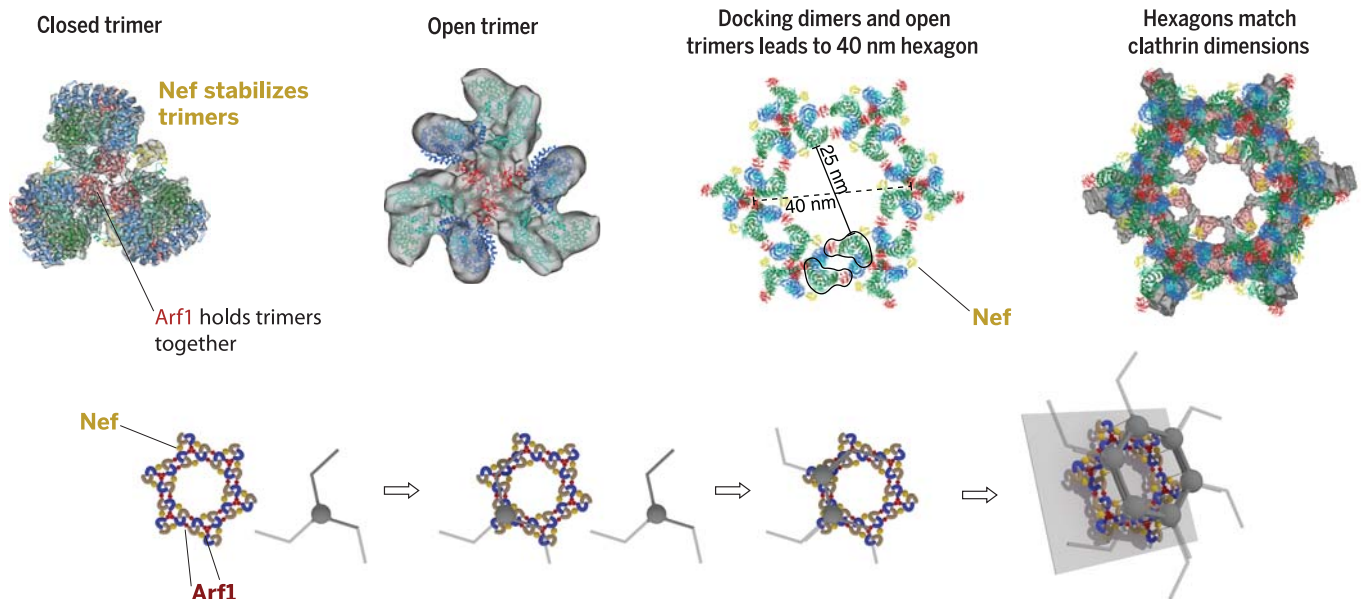
Read the full article at <http://dx.doi.org/10.1126/science.aac5137>

AP-1:Arf1:MHC-I-Nef mixtures. Efficient clathrin cage assembly at neutral pH required Nef and intact Arf1 dimer and trimer interfaces.

CONCLUSION: Although we set out to explain how HIV-1 Nef hijacked the AP-1 complex, we also found that the inner layer of the AP-1 clathrin coat is far more intricately organized than anticipated. AP-1 and its Arf1 binding sites are conserved throughout eukaryotes; thus, the organization of the inner layer is ancient. HIV-1 has taken advantage of this complexity to subvert membrane traffic. The degree to which HIV-1 Nef can drive AP-1 hexagon formation seems to be coupled to its cargo preferences, as Nef recruits MHC-I more effectively than tetherin. Our findings elucidate the structured organization of the inner layer of clathrin coats that is conserved across eukaryotes, as well as the means by which HIV-1 uses Nef to subvert this structure. ■

The list of author affiliations is available in the full article online.
*These authors contributed equally to this work.
†Corresponding author. E-mail: jimhurley@berkeley.edu
Cite this article as Q.-T. Shen *et al.*, *Science* 350, aac5137 (2015). DOI: 10.1126/science.aac5137

HIV-1 Nef, Arf1, and the hexagonal inner layer of an AP-1 clathrin coat. (Top) Cryo-EM reconstructions of closed (far left) and open (center left) trimers of tetherin-HIV-1 Nef fusion protein, Arf1, and the AP-1 core. Combining the open trimer and known dimer structure leads to a hexagonal model (center right) that matches the dimensions of the clathrin coat (right). (Bottom) Concept for Nef-activated assembly of the AP-1-clathrin coat.



RESEARCH ARTICLE

CLATHRIN ADAPTORS

HIV-1 Nef hijacks clathrin coats by stabilizing AP-1:Arf1 polygons

Qing-Tao Shen,^{1*} Xuefeng Ren,^{1*} Rui Zhang,^{2*} Il-Hyung Lee,¹ James H. Hurley^{1,2†}

The lentiviruses HIV and simian immunodeficiency virus (SIV) subvert intracellular membrane traffic as part of their replication cycle. The lentiviral Nef protein helps viruses evade innate and adaptive immune defenses by hijacking the adaptor protein 1 (AP-1) and AP-2 clathrin adaptors. We found that HIV-1 Nef and the guanosine triphosphatase Arf1 induced trimerization and activation of AP-1. Here we report the cryo-electron microscopy structures of the Nef- and Arf1-bound AP-1 trimer in the active and inactive states. A central nucleus of three Arf1 molecules organizes the trimers. We combined the open trimer with a known dimer structure and thus predicted a hexagonal assembly with inner and outer faces that bind the membranes and clathrin, respectively. Hexagons were directly visualized and the model validated by reconstituting clathrin cage assembly. Arf1 and Nef thus play interconnected roles in allosteric activation, cargo recruitment, and coat assembly, revealing an unexpectedly intricate organization of the inner AP-1 layer of the clathrin coat.

Vesicular coats are involved in intracellular membrane traffic and are central to the organization of eukaryotic cells (1). Coats consist of (i) a structural scaffold and (ii) adaptor elements that link the scaffold to membrane proteins and lipids. The scaffold and adaptor may exist as separate layers, or they may be combined. Clathrin is the archetypal two-layer vesicular coat (2) and is responsible for much of the vesicular traffic originating at the plasma membrane and trans-Golgi network (TGN), as well as intraendosomal traffic. The clathrin heavy and light chains form the scaffold, and the heterotetrameric adaptor protein (AP) complexes are the most prevalent adaptor components for clathrin (3, 4). Clathrin does not bind directly to cargo or membranes; rather, the AP complexes connect cargo and membranes to clathrin. The AP-1 complex functions at the TGN, where it is recruited and activated by the small guanosine triphosphatase (GTPase) Arf1 (ADP-ribosylation factor 1) (5, 6). AP-1 consists of two large subunits (β 1 and γ), a medium subunit (μ 1), and a small subunit (σ 1) (3). The large subunits contain flexibly tethered C-terminal ear domains, and constructs lacking the linkers and ears are referred to as AP cores. AP-1 cargoes contain either tyrosine-based sorting signals, which bind to the C-terminal domain (CTD) of μ 1, or dileucine signals, which bind to a site spanning the γ and σ 1 subunits (4). The activity of AP complexes is tightly regulated, and in the absence of activation, the cargo binding sites are sequestered in a state known as the locked conformation (7, 8). AP-1 is “unlocked” by

Arf1-GTP through an allosteric mechanism coupled to the formation of a 2:2 AP-1:Arf1 dimer (9).

The lentiviruses HIV-1, HIV-2, and simian immunodeficiency virus (SIV) hijack the clathrin pathway via their accessory proteins Nef (negative factor) and Vpu (viral protein unique) (10, 11). Lentiviral hijacking facilitates viral immune evasion, assembly, and release by down-regulating cell surface receptors and restriction factors, including CD4 (cluster of differentiation 4) (12, 13), major histocompatibility complex I (MHC-I) (14), and tetherin (15). AP-1 mediates the ability of Nef and Vpu to reroute MHC-I and tetherin from the plasma membrane to lysosomes (16, 17). Nef hijacks AP-1 to down-regulate MHC-I via the tyrosine motif binding site on the CTD of μ 1 (18), whereas AP-2 is hijacked to down-regulate CD4 via the dileucine binding site on the α -2 complex (19, 20). Both Nef binding sites are occluded in the locked conformation (21, 22). Nef subversion of membrane traffic thus requires that AP complexes be unlocked. One report has suggested that Nef can drive membrane localization of AP-1 independent of Arf1 (23), whereas another found that Nef stabilizes the AP-1 coat only in the presence of Arf1 (24) and a third showed that Arf1 is required for Nef-driven down-regulation of MHC-I (25). Along with the subunits of AP-1 and MHC-I, Arf1 is one of ~50 Nef-interacting proteins detected in the human proteome (26). We set out to determine whether Nef, in combination with host cargo, could either bypass or amplify the endogenous Arf1-dependent unlocking mechanism.

HIV-1 Nef and Arf1 trimerize AP-1

We fused the cytosolic 21 amino acids of tetherin, which bind tightly to AP-1 (17), to full-length HIV-1 NL4-3 Nef. We co-incubated tetherin-Nef, the AP-1 core (henceforward referred to as AP-1), and the GTP-locked and N-terminally truncated

Arf1 mutant Gln⁷¹→Leu⁷¹ (Q71L) (27) (henceforward Arf1). These molecules formed a complex that had a molecular weight of 850 kD, as determined by multiangle light scattering (MALS) (Fig. 1, A and B). This value corresponds to three AP-1:Arf1:tetherin-Nef complexes. In contrast, the AP-1 complex alone migrated at a mass consistent with that of a single heterotetramer (Fig. 1B). AP-1:Arf1 contained two peaks, with the higher-mass peak corresponding to a species with a known dimeric crystal structure (9) (Fig. 1A). Other combinations of AP-1, Arf1, and Nef in the presence or absence of a physiological cargo peptide (TGN38) or fused to the tail of MHC-I were also tested. These complexes manifested an apparent mixture of monomer, dimer, and trimer, or in the case of MHC-I, a heterogeneous mixture of higher-order species (Fig. 1A and fig. S1).

The AP-1:Arf1:tetherin-Nef trimers appeared to be promising for structural characterization on the basis of their monodispersity. To determine whether these trimers corresponded to the unlocked conformation, we developed a Förster resonance energy transfer (FRET) reporter for AP-1 unlocking (Fig. 1, C and D). In the locked conformation (28), the separation between β 1-E471 and μ 1-K333 was 17 Å, whereas the distance increased to 58 Å in both the unlocked (9) and the even more open hyperunlocked (17) conformations (Fig. 1D). We constructed an AP-1 variant in which all 34 native Cys residues were replaced by Ala. The mutation β 1E471C μ 1K333C was generated in the Cys-free context and fluorescently labeled with Cy3 and Cy5. The labeled AP-1 formed the same 850-kD complex with tetherin-Nef and Arf1, so we compared the spectra of the labeled AP-1 alone and in complex with tetherin-Nef and Arf1 (Fig. 1C). The spectra indicated a loss of FRET in the presence of tetherin-Nef and Arf1, consistent with AP-1 unlocking.

Cryo-EM reconstruction of AP-1:Arf1:tetherin-Nef trimers

We collected negative-stain and cryo-electron microscopy (cryo-EM) images for the gel filtration peak corresponding to the 850-kD complex and carried out two-dimensional (2D) and 3D classifications (Fig. 2A and figs. S2 and S3). The complex consisted of two different types of trimers, with a small proportion of dimers (Fig. 2, A and B). Roughly 24% of the population consisted of trilobed particles, whereas ~72% corresponded to triangles. The reconstruction of the trilobed particles was improved by masking a subassembly to yield a 7 Å reconstruction (Fig. 2, C and D; figs. S4 and S5; and movie S1). The density was readily interpretable, and three crystal structures—one copy of the hyperunlocked conformation of AP-1 (17); one copy of Nef in the conformation bound to the μ 1 CTD (21); and two Arf1 molecules, as bound to β 1 (Arf1 ^{β}) (9) and to the coatamer [coat protein complex I (COPI)] counterpart of γ (Arf1 ^{γ}) (29)—easily docked into each of the three lobes (fig. S5). These molecules collectively accounted for essentially all of the density (Figs. 2D and 3A).

Arf1 ^{γ} and Arf1 ^{β} contacted AP-1 via their GTP-responsive switch I and II (SwI/II) regions,

¹Department of Molecular and Cell Biology and California Institute for Quantitative Biosciences, University of California, Berkeley, Berkeley, CA 94720, USA. ²Life Sciences Division, Lawrence Berkeley National Laboratory, Berkeley, CA 94720, USA.

*These authors contributed equally to this work. †Corresponding author. E-mail: jimhurley@berkeley.edu

consistent with the GTP-dependence of Arf1 activation of AP-1 (Fig. 3B). The region of Arf1^Y comprising residues H80, Q83, E113, D114, and E115 (outside the SwI/II regions) contacts the tip of the cargo-binding μ 1 CTD (Fig. 3C). This part of the μ 1 CTD moves ~ 27 Å from its position in the conventional unlocked structure to make these contacts. These μ 1-CTD contacts with Arf1 presumably help drive the hyperunlocked conformation in the Arf1-linked trimer. The trimer is held together in part by direct contacts between three copies of Arf1^Y. The N175-R178 region and the C-terminal K181 of one Arf1 molecule contact the H146-W153 region and the Q176-N179 residues

of the next Arf1 (Fig. 3D). Arf1 is not known to trimerize in isolation, and we surmise that either (i) AP-1 promotes a distinct conformation of Arf1 that is prone to trimerization or (ii) additional contacts elsewhere in the assembly cooperate to promote the trimer. With respect to (i), at 7 Å resolution it is not possible to determine whether AP-1 induces subtle conformational changes in Arf1. With respect to (ii), a major interleaf bridge that stabilizes the trimer is formed by a contact between the N termini of Nef and β 1 (Figs. 2D and 3E). This trimer structure sequesters the cargo-binding site of the three μ 1 CTDs such that they face the center of the trimer; hence, mem-

brane interactions are precluded. Even though the individual AP-1 complexes are in the hyperunlocked conformation, the overall trimer is closed (Fig. 3F). Thus, we refer to this minority population of trimers as “closed” and conclude that this state would be inactive for vesicle formation.

The majority population of triangle-shaped particles yielded a 17 Å reconstruction (Fig. 4A, figs. S6 to S8, and movie S2). The resolution was limited by heterogeneity in the position of the three monomers within the triangle, which visibly contact one another only in the center. The density can be reasonably explained by docking three copies of the monomeric AP-1:Arf1^Y unit of the closed-state model described above (Fig. 4A). Each AP-1:Arf1^Y complex was docked as a rigid body while maintaining the central nucleus of three Arf1^Y molecules. Owing to the mobility of the monomers, we could not visualize clear density for Nef or Arf1^B, although Nef was stoichiometrically bound in the sample (Fig. 1A). The C termini of the β 1 subunit come into close approach at the center. In this structure, the tyrosine and dileucine binding sites, the myristoylation site at the N terminus of Arf1, and the phosphatidylinositol 4-phosphate binding site of AP-1 fall into an approximate plane (Fig. 4B). Because all of the sites are accessible, we refer to this state as “open.”

AP-1:Arf1 hexagonal rings

A previous crystal structure of a 2:2 unlocked AP-1:Arf1 complex solved in the absence of Nef and cargo led to a model for Arf1 activation in the context of a dimeric assembly (9). In that structure, the SwI/II Arf1^B contact was present, and a second contact was made between W172 of the back side of Arf1^B and the α 12- α 16 region of the γ subunit (Fig. 4C). The mutation W172D prevents Arf1 from activating AP-1, which validated the role of the dimer contact in activation. This finding prompted us to consider the relation between the previous dimer and the current trimer structure. In the open trimer structure, the Arf1^B site and γ - α 12- α 16 are unobstructed and aligned in a plane parallel to the membrane. We docked the dimeric crystal structure onto these sites (Fig. 4C). Iterative docking of the dimers and trimers linked by Arf1^B bridges generated a hexagonal ring consisting of 18 AP-1 complexes and 36 Arf1 molecules (Fig. 4D). The

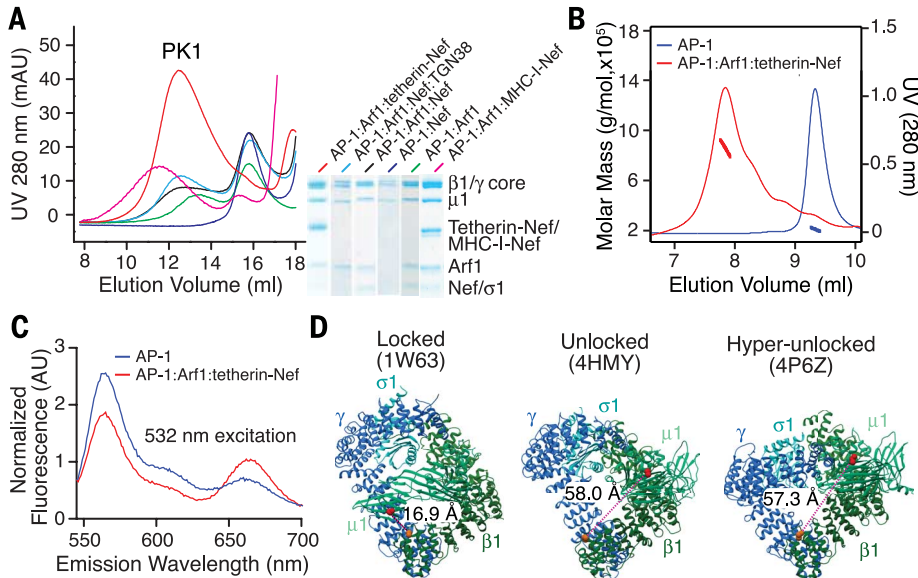


Fig. 1. Arf1, cargo, and Nef trimerize and unlock AP-1. (A) Size exclusion chromatography of AP-1 complexes. Partners are indicated with color codes at right. Peak 1 (PK1) indicates the high-molecular weight AP-1:Arf1:tetherin-Nef complex, whose central fraction was used for subsequent biophysical and cryo-EM studies. The gel shown at right was loaded with samples from PK1 for AP-1:Arf1:tetherin-Nef, and the highest-molecular weight peak eluted for each of the other samples tested. UV, ultraviolet; mAU, milliabsorbance units. (B) Multiangle light scattering (MALS) of AP-1:Arf1:tetherin-Nef (red) and free AP-1 (blue). (C) Emission spectra of free AP-1 and the AP-1:Arf1:tetherin-Nef complex, with excitation at 532 nm. The increase in Cy3 emission and the decrease in Cy5 emission illustrate the FRET efficiency decreases in the complex. The original intensity counts were normalized by the estimation of the total Cy5 amount. AU, arbitrary units. (D) Distance changes anticipated between the locked and unlocked AP-1 complexes, obtained from the indicated PDB entries. The distance increase from 17 to 58 Å corresponds to a twofold decrease in FRET efficiency difference for the Cy3-Cy5 pair ($R_0^6 = 60$ Å) and $E = R_0^6 / (R_0^6 + R^6)$ (R , distance between fluorophores; E , FRET efficiency).

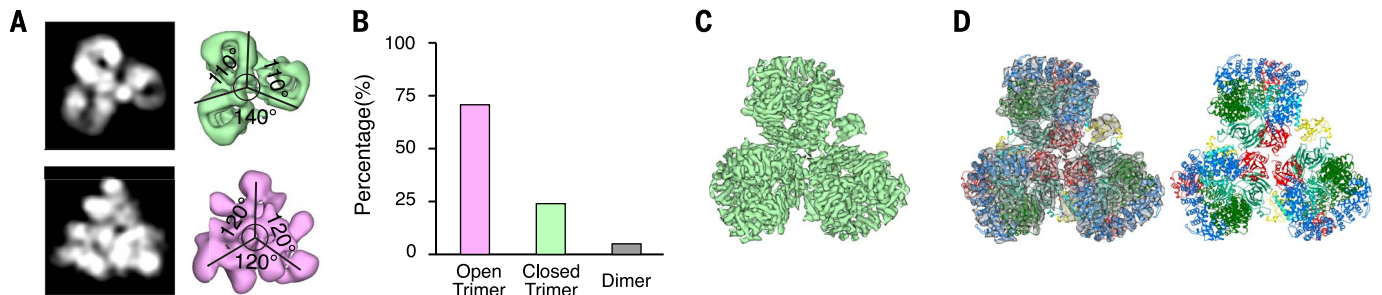


Fig. 2. Cryo-EM reconstruction of two types of AP-1:Arf1:tetherin-Nef trimers. (A) Representative 2D and 3D classes of trimers. (B) Relative populations of dimers and closed and open trimers. (C) Submasking and 7 Å reconstruction of a subassembly of the closed trimer. (D) Overall view of the docking of the hyperunlocked AP-1 structure, Arf1, and Nef into the closed trimer reconstruction.

ring is essentially identical in diameter to the hexagons seen in the cryo-EM reconstruction of the clathrin cage (30) (Fig. 4E). The clathrin binding sequence of the $\beta 1$ subunit is located directly under the projections of the clathrin density corresponding to the clathrin terminal domain (Fig. 4F). Thus, the AP-1:Arf1 hexagon is in almost perfect alignment to template the recruitment and organization of clathrin.

Spurred by this model, we revisited the high-molecular weight tail of the polydisperse AP-1:Arf1:MHC-I-Nef sample (Fig. 1A and fig. S9). We had originally considered this material too heterogeneous for EM analysis, even though MHC-I is the best known substrate for HIV-1 Nef down-regulation via AP-1. The earliest-eluting fractions of this material were subjected to negative-stain EM (Fig. 5A). We observed an abundance of polygons, including a substantial population of closed hexagons, with dimensions that were consistent with the mode of oligomerization suggested by the model. To quantitate the relative numbers of different particles, we subjected them to 2D class averaging (Fig. 5A). The particles were not perfectly identical, so the class averages lost density near the edges. Nevertheless, when atomic models were superimposed on the raw images, convincing fits were obtained (Fig. 5B).

Clathrin cage assembly promoted by AP-1 hexagons

To validate the Arf1-mediated dimer and trimer interfaces, we constructed Arf1 mutants in the

SwI region (I49D) (31), the dimer contact with the back side of Arf1^P (W172D) (9), and the two regions involved in the central trimer contacts (Fig. 5C). All of these mutants were stable and purified in isolation as monomers (fig. S10). We then tested their ability to oligomerize in the context of the AP-1:Arf1:unfused Nef complex. The wild-type (WT) complex runs as a mixture of trimer and higher-order species (Fig. 5D). No isolated dimeric species was seen in the size exclusion chromatography (SEC) of this complex, but the higher-order species were presumed to arise via a combination of dimer and trimer interactions. The dimer interface mutant W172D yields a sharper trimer peak and reduces the proportion of higher-order species (Fig. 5D). The SwI mutant I49D and the trimer-interface loop replacement Arf1 ^{Δ 148-152GS} completely eliminate the trimer and larger species. The C-terminal deletion Arf1 ^{Δ 178-181} reduces but does not eliminate the trimer. These findings are all consistent with the observed set of structural contacts.

We went on to reconstitute clathrin cages in vitro (Fig. 5E) to determine whether the formation of Nef- and Arf1-promoted polygons in turn led to clathrin assembly. WT Arf1 and Nef supported efficient cage assembly (Fig. 5F). In contrast, the SwI and dimer mutants and one of the trimer interface mutants had near-background levels of cage assembly (Fig. 5F). The second trimer interface mutant, the deletion of the C-terminal four residues, had a modest effect of marginal importance (Fig. 5F). The limited effect of this

mutant is consistent with the modest reduction in the trimer peak seen in Fig. 5D. Thus, the Arf1 bridges that hold the dimer and trimer together are essential for the promotion of clathrin cage assembly.

We mutated key residues in Nef contacts with AP-1 to probe their role in the activation of clathrin cage formation. Nef is capable of binding to the γ - $\sigma 1$ hemicomplex of AP-1 via its dileucine motif (32) (Fig. 6A). The dileucine- γ - $\sigma 1$ interaction is not essential for down-regulation of MHC-I by AP-1, and Nef is not visualized at this site in the EM density. Nevertheless, we reasoned that WT Nef can still bind to this site and could promote AP-1 unlocking. We tested the ability of Nef^{LL164-165AA} and MHC-I-Nef^{LL164-165AA} to promote AP-1 oligomerization and clathrin cage assembly. In the presence of Nef^{LL164-165AA}, AP-1 and Arf1 migrated as if Nef were absent (Fig. 6B), and clathrin cage assembly was reduced to the same background level seen without Nef (Fig. 6C). MHC-I and tetherin cooperate with Nef to bind to the $\mu 1$ CTD via an interface that does not involve the dileucine motif but does involve Asp¹²³ (21). This is the site that is well ordered in the EM density of the closed trimer in the presence of cargo. MHC-I-Nef^{LL164-165AA} still trimerizes AP-1 (Fig. 6D), although the presence of higher-order oligomers was reduced. MHC-I-Nef^{LL164-165AA} promotes clathrin cage assembly (Fig. 6E) with efficiency relatively near that of the wild type, consistent with the biological finding that MHC-I down-regulation does not require the dileucine motif (33). Conversely, MHC-I-Nef^{D123R}, which destabilizes the $\mu 1$ -CTD interface, decreased the proportion of trimeric AP-1 (Fig. 6D) and reduced clathrin cage assembly to ~30% of WT levels (Fig. 6E). In the absence of MHC-I, Nef^{D123R} displayed near-WT oligomerization (Fig. 6B) and cage assembly behavior (Fig. 6C), consistent with the dependence of the Nef- $\mu 1$ -CTD interaction on the presence of $\mu 1$ -CTD-directed cargo (21).

Conclusions

Previous models of AP-mediated clathrin recruitment have emphasized the plasma membrane adaptor AP-2, which is activated principally by phosphatidylinositol 4,5-bisphosphate, not Arf1 (34). In the reconstruction of an AP-2 clathrin coat, the AP-2 complexes were disordered and substoichiometric (30). The recruitment of clathrin to the plasma membrane appears to be coupled to recruitment of AP-2 complex pairs (35) rather than a larger scaffold. Our contrasting observations of an ordered inner layer for AP-1 point to a fundamental difference between the AP-1 and AP-2 coats. Our findings for AP-1 will likely also apply to the Arf1-activated AP-3 adaptor complex. In a very recent cryo-EM tomographic study of COPI vesicles, Dodonova *et al.* noted Arf1-mediated trimers similar to those seen here (36). In other ways, the two-layer hexagonal organization described here for AP-1 and clathrin differs from the interwoven assembly of COPI. In summary, our results show that the inner layer of the AP-1 clathrin coat, and probably other Arf1-dependent clathrin coats, has a far more

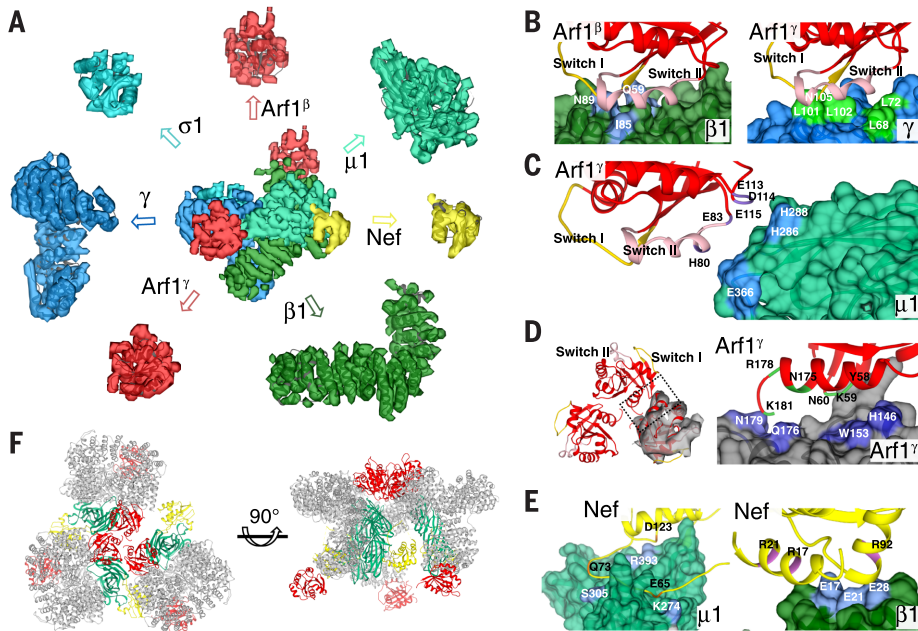


Fig. 3. Molecular interactions in the closed AP-1:Arf1:tetherin-Nef trimer. (A) Exploded view of subunit-by-subunit fits into the closed trimer reconstruction. (B) Details of interactions between Arf1 and the $\beta 1$ and γ subunits. (C) Interactions between Arf1 and the $\mu 1$ CTD drive hyperunlocking. (D) Interactions at the center of the Arf1 nucleus stabilize the trimer. (E) Interactions between Nef and the $\mu 1$ CTD (left) mirror those seen previously (21), whereas a distinct trimer-bridging interaction is observed between Nef and the N terminus of $\beta 1$ (right). (F) The closed AP-1:Arf1:tetherin-Nef trimer. The reported membrane and cargo binding subunits including Arf1, $\mu 1$, and Nef are illustrated with the same colors used previously, whereas the other parts are shown in gray.

organized structure than previously appreciated. Moreover, Arf1 plays a far more central role than previously understood. Not only does Arf1 drive recruitment and allosteric activation of AP-1, but it is also an integral component of the structure of the inner layer, bridging the individual AP-1 complexes into dimers and trimers and thence to hexagons.

The highly organized inner-layer structure introduces an additional level at which regulation can occur. HIV-1 Nef appears to take advantage of the additional complexity by promoting trimer formation, which could allow it to template clathrin cages under conditions that would otherwise fall short of full activation (Fig. 6F). Trimer promotion appears to occur by both indirect and direct mechanisms. The structural observation that Nef can bridge between different AP-1 complexes within the trimer suggests that Nef can also drive trimerization directly. The loss of function for Nef^{ΔLL164-165AA} in the absence of MHC-I is consistent with an indirect mechanism, wherein Nef binds tightly to γ - σ 1 (32), driving the thermodynamic equilibrium toward the unlocked state, which in turn is capable of forming a trimer.

We currently believe that these two mechanisms can work either alone or together in different contexts.

MHC-I-Nef is much more effective than tetherin-Nef at promoting polygon formation, even though both constructs bind tightly to AP-1. HIV-1 NL4-3 (the source of Nef used in this study and a member of group M) down-regulates MHC-I via Nef and tetherin via Vpu. However, HIV group O, like SIV, uses Nef to down-regulate tetherin (37). Perhaps HIV-1 O-Nef and SIV Nef might be more effective than HIV-1 NL4-3 or other M- and N-Nefs at promoting polygon formation in the presence of tetherin. If confirmed, this would provide a molecular mechanism for virus-specific differences in the mode of tetherin down-regulation.

Our observations of the ordered inner layer of the AP-1 clathrin coat were made in the stabilizing presence of HIV-1 Nef and cargo. The conservation of the Arf1-binding sites in the evolution of AP-1 from yeast to humans leaves little doubt that the ordered inner layer is far more ancient than the appearance of the primate lentiviruses. The elaborate organization of the AP-1:Arf1 inner layer

might offer advantages to the cell in terms of clathrin assembly speed, regulatory versatility, or both. Clathrin coats can be generated on synaptic endosomes within a span of 2 s (38), a pathway that most likely involves the Arf1-activated AP-1 and/or AP-3 complexes. Cooperative assembly of a symmetry-matched hexagonal inner layer would be a clear asset in catalyzing the rapid nucleation of an endosomal clathrin coat. These benefits could have been adaptive early in the evolution of eukaryotes.

Materials and methods

Plasmid construction

The His₆- and glutathione *S*-transferase (GST)-tagged AP-1 core expression construct was described by Ren *et al.* (9). In the variant FL β :AP-1 complex used for clathrin assembly experiments, β 1 (residues 1 to 584) was replaced with full-length β 1 DNA. A tobacco etch virus (TEV) cleavage site and His₆ tag were fused to the C terminal of full-length β 1. To generate the Cys-free construct, DNAs encoding the AP-1 core subunits were codon-optimized and synthesized (Genescript, Piscataway, NJ). The Cys-free (C2A) construct was then used as a template for site-directed mutagenesis to produce the desired Cys pair construct. HIV-1 NL4-3 Nef, tetherin (1 to 21)-10 amino acid linker-Nef, and MHC-I (338 to 365)-Nef were expressed as TEV-cleavable N-terminal His₆ fusions. His₆-tagged full-length Nef was used for clathrin cage assembly. The N-terminal truncation of Nef (56 to 206) was used for SEC of AP1:Arf1:Nef trimer complexes. Human Arf1 (17 to 181) Q71L or other Arf1 mutants made in this background were expressed with a TEV-cleavable N-terminal His₆ tag.

Protein expression and purification

The AP-1 complexes were expressed in BL21 (DE3) Star (Life Technologies, Grand Island, NY) or BL21 (DE3) pLysS (Promega, Madison, WI) strains and induced with 0.3 mM isopropyl- β -D-thiogalactopyranoside (IPTG) at 20°C overnight. The cells were lysed by sonication in 50 mM Tris at pH 8.0, 300 mM NaCl, 10% glycerol, 3 mM β -mercaptoethanol (β -ME), and a protease inhibitor cocktail (Sigma-Aldrich, St. Louis, MO). The clarified lysate was first purified on a Ni-nitrilotriacetic acid (NTA) column (QIAGEN, Valencia, CA). The eluate was further purified on glutathione-Sepharose 4B resin (GE Healthcare, Piscataway, NJ). After TEV cleavage at 4°C overnight, the sample was concentrated and then loaded onto a HiLoad 16/60 Superdex 200 column (GE Healthcare) in 20 mM Tris at pH 8.0, 200 mM NaCl, and 0.3 mM tris(2-carboxyethyl)phosphine (TCEP). The sample fractions were pooled together, adjusted to 30 mM imidazole, and passed through 1 ml of glutathione-Sepharose 4B and then onto a Ni-NTA column (QIAGEN) to capture the residual GST- and His-tag fragments. The sample was adjusted to 20 mM Tris at pH 8.0, 200 mM NaCl, and 0.3 mM TCEP by buffer exchange in the concentrator.

His₆-tagged tetherin-Nef and other Nef constructs were expressed in BL21 (DE3) Star cells

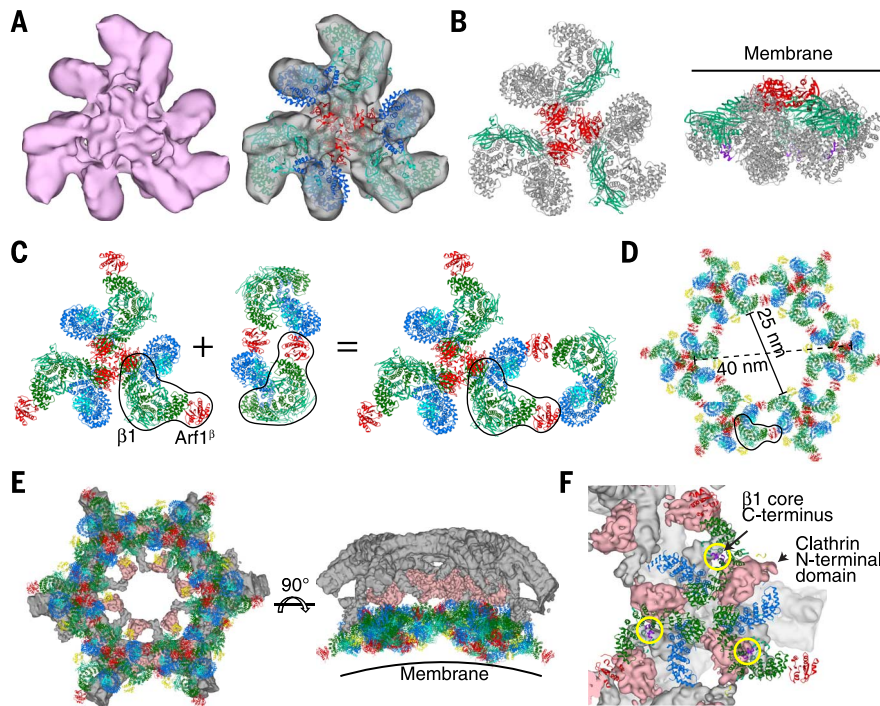


Fig. 4. The open AP-1:Arf1:tetherin-Nef trimer suggests a hexagonal assembly model. (A) Reconstruction and docking of the open AP-1:Arf1:tetherin-Nef trimer. (B) The open AP-1:Arf1:tetherin-Nef trimer. The reported membrane and cargo binding subunits including Arf1, μ 1, and Nef are colored as before, whereas the other parts are shown in gray. The membrane is represented by a horizontal line. The C terminus of the β 1 core, which is the location of the clathrin binding region, is shown in purple. (C) The open AP-1:Arf1 trimer formed in the presence of Nef (left) and the known Nef-free AP-1:Arf1 dimer (to the right of the plus sign) (9) were docked onto one another by overlaying one copy each of the β 1 subunit and Arf1 β (outlined in black) to yield the composite structure at far right. (D) Iterating the docking operation shown in (C) generates the hexagon illustrated here. Nef was docked onto all copies of AP-1 in the mode identified in the closed trimer and is shown in yellow. (E) Juxtaposition of the modeled hexagon and one hexagonal segment of the cryo-EM reconstruction of the clathrin D6-barrel (30). The membrane binding face is represented by a curved line. (F) A close-up view of the hexagon model and the clathrin D6-barrel density shows that the clathrin binding site on β 1 adjoins the AP-1 binding site on clathrin.

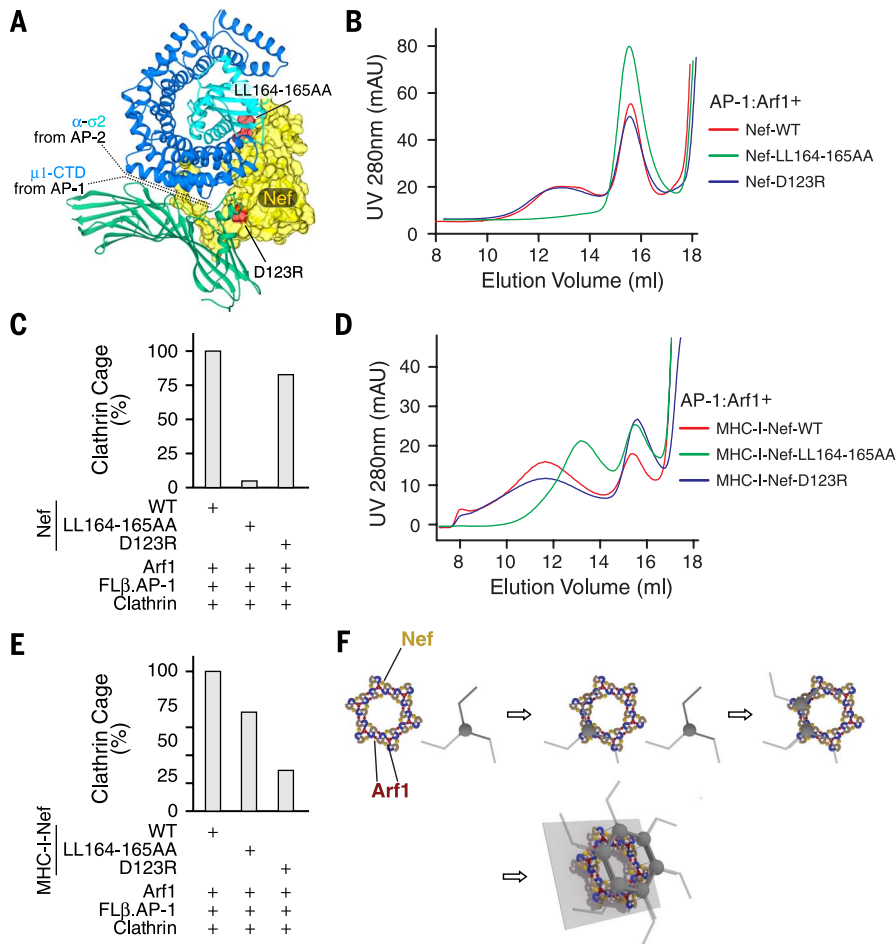


Fig. 6. The hexagonal inner coat promotes clathrin cage assembly. (A) Diagram of Nef mutants. Structures from AP-2- α -2:Nef (PDB ID 4NEE) and AP-1- μ 1:MHC-I-Nef (PDB ID 4EMZ) were combined. Homologs are colored as before. (B) Size exclusion chromatography of AP-1:Arf1:Nef mixtures, showing that Nef mutants interfere with dimerization or trimerization of AP-1. (C) The relative percentage of clathrin cages was counted in 20 randomly chosen fields of view for the indicated mixtures of WT and/or mutant Nef proteins. (D) Size exclusion chromatography of AP-1:Arf1:MHC-I-Nef mixtures, showing that MHC-I-Nef mutants interfere with dimerization or trimerization of AP-1. (E) The relative percentage of clathrin cages was counted in 20 randomly chosen fields of view for the indicated mixtures of WT and/or mutant MHC-I-Nef proteins. (F) Concept for the role of AP-1:Arf1 polygons in clathrin assembly with Nef. Nef (yellow) stabilizes the AP-1:Arf1 polygon such that closed polygons can form even without clathrin, creating a preformed template for rapid clathrin assembly.

were adjusted to total protein concentrations of 0.02 mg/ml for negative-stain EM. Four-microliter droplets of the sample were placed on glow-discharged carbon-coated copper grids and were negatively stained using 2% (w/v) uranyl acetate. For clathrin-related samples, we allowed an extra 5 min of incubation time on the grid with 3% glutaraldehyde to fix clathrin cages before the application of uranyl acetate, as described previously, with minor modifications (39). Negatively stained samples were examined under a Tecnai F20 microscope (FEI, Eindhoven, Netherlands) operated at an accelerating voltage of 120 keV with a defocus from -1.0 to -1.5 μ m at tilts of 0° or 45° . Micrographs were recorded on a charge-coupled device camera (Ultrascan 4000, 4 k \times 4 k; Gatan, Pleasanton, CA) at a nominal magnifica-

tion of 80,000 \times with a 1.37 \AA calibrated pixel size at the specimen level, using the semiautomated Legikon data collection software (40).

Cryo-EM

Droplets of 2.5- μ l AP-1, Arf1, and the tetherin-Nef complex sample at a concentration of 0.06 mg/ml were applied to Quantifoil grids with continuous carbon support and plunge frozen into liquid ethane using a Vitrobot Mark IV (FEI). The vitrified samples were examined using a Titan microscope (FEI) operated at 300 keV. The vitrified samples were imaged under parallel illumination conditions, with a beam diameter of ~ 2 mm on the specimens and a defocus range from -1.5 to -3.5 μ m. All cryo-EM images were recorded on a K2 Summit direct electron detector camera

(Gatan) at a nominal magnification of 27,500 \times , corresponding to a calibrated pixel size of 1.32 \AA . The camera was operated in counting mode, with a dose rate of about eight electrons per pixel per s on the camera. A total exposure time of 10 s, corresponding to an accumulated dose of 45.9 electrons/ \AA^2 on the specimen, was fractionated into 25 movie frames, with 0.4-s exposure time and a dose of 1.84 electron/ \AA^2 for each frame. The data were collected semiautomatically, using the Legikon data collection software (40). Drift correction for movie frames was performed using the University of California, San Francisco (UCSF) MotionCorr program (41). The parameters of the contrast transfer function (CTF) were estimated from the drift-corrected micrographs using CTFIND4 (<http://grigoriefflab.janelia.org/ctffind4>).

Image processing

The program XMIPP/3.1 was used for 2D analysis and random conical tilt (RCT) analysis of negatively stained samples (42). A total of 11,589 untilted and tilted particle pairs was manually selected from 176 micrograph pairs. The untilted image stack was subjected to reference-free 2D classification (50 classes) (43). For 38 representative classes, the corresponding tilted particle images were used to compute 3D reconstructions via the RCT approach (44). The obtained 3D reconstructions were classified into three groups (open triangles, closed three-leaf clover, and dimer-like) by visual inspection. Both untilted and tilted particles corresponding to each trimeric shape were combined and used to generate a final structure based on projection match. The final resolutions for the open and closed trimers were determined to be 27 and 26 \AA , respectively, based on the 0.5 criterion of the Fourier shell correlation (FSC).

Further cryo-EM data analysis of images obtained from the Titan microscope was performed using the RELION/1.4-beta-1 program (45). Particles were picked from 1445 drift-corrected micrographs using the DoG Picker software (46) inside the APPION image processing suite (47), and the particle coordinates were transferred to RELION for particle extraction. A total of 144,261 individual particles were subject to reference-free 2D classification (using 100 classes) to remove poor-quality particles. The remaining data set comprising 111,183 particles was used for further analyses. With the RCT structure low-pass filtered to 60 \AA as an initial model, we performed 3D classification with 10 classes, which, after 50 iterations, revealed two major conformations: closed (one class) and open trimers (eight classes). Further 3D classification of the closed class (26,069 particles) into five subclasses revealed that the third subunit is wobbling with respect to the other two subunits (fig. S5D). The flexibility of the third subunit limited the refinement resolution of the whole trimer to 9.0 \AA . To improve the resolution of the round-edge class, we masked the third subunit during the autorefinement process and produced a reconstruction for the two rigid subunits at 8.1 \AA . A similar strategy to mask only one subunit from the trimer during autorefinement

further improved the resolution to 7.0 Å. The other eight open-state classes were reorganized into four classes, and 32,535 particles were selected for the subsequent autorefinement process. Due to the sample heterogeneity, the refinement was limited to 23.8 Å resolution. All classes superimpose reasonably well with respect to each other, revealing an apparent C3 symmetry, at least at low-to-medium resolution. Therefore, we enforced C3 symmetry during the refinement, which resulted in a final resolution of 16.7 Å. All reported resolutions for the RELION reconstruction are based on the gold standard 0.143 FSC criterion, using two independent half-maps, with correction of the effects from the soft-edged mask. The angular distribution of each structure was also calculated with the RELION package.

Docking and structural analysis

Crystal structures of the hyperunlocked AP-1 core bound to tethrin [Protein Data Bank identification code (PDB ID) 4P6Z] (17), the unlocked AP-1 core with Arf1 (PDB ID 4HMY) (9), and the closed AP-1 core (PDB ID 1W63) (28) were used as trial structures for docking. The docking was fulfilled in UCSF Chimera on the basis of a rigid-body docking strategy (48). In closed trimer, the crystal structure of hyperunlocked AP-1 fit well into the EM density map as an intact unit. Most of the α helices of the β and γ subunits in AP-1 were clearly visualized in the density, and the β sandwich of the μ 1 subunit also fit well in the density. In addition to densities occupied by AP-1 core, two of the three unassigned EM densities were identified as Arf1 (PDB ID 1O3Y) (49), based on excellent matching of α helices with the EM densities. The third unoccupied EM density lies close to the μ 1 domain and was docked well using Nef (PDB ID 4EMZ), which is further verified by the known interface between AP-1:Arf1:Nef (9) and the solved structure of the μ 1 domain, Nef, and MHC-I (21). Hyperunlocked AP-1 with Arf1^Y fit into the EM density map for the open trimer, with or without C3 symmetry, as an intact unit. Preliminary docking results were selected from 500 random placements with the best cross-correlation values and the most hits. The possible candidates were further screened on the basis of both symmetrized C3 docking and the position of Arf1^Y in the EM density.

REFERENCES AND NOTES

- R. Schekman, L. Orci, Coat proteins and vesicle budding. *Science* **271**, 1526–1533 (1996). doi: [10.1126/science.271.5255.1526](https://doi.org/10.1126/science.271.5255.1526); pmid: 8599108
- T. Kirchhausen, Clathrin. *Annu. Rev. Biochem.* **69**, 699–727 (2000). doi: [10.1146/annurev.biochem.69.1.699](https://doi.org/10.1146/annurev.biochem.69.1.699); pmid: 10966473
- D. J. Owen, B. M. Collins, P. R. Evans, Adaptors for clathrin coats: Structure and function. *Annu. Rev. Cell Dev. Biol.* **20**, 153–191 (2004). doi: [10.1146/annurev.cellbio.20.010403.104543](https://doi.org/10.1146/annurev.cellbio.20.010403.104543); pmid: 15473838
- L. M. Traub, J. S. Bonifacino, Cargo recognition in clathrin-mediated endocytosis. *Cold Spring Harbor. Perspect. Biol.* **5**, a016790 (2013). doi: [10.1101/cshperspect.a016790](https://doi.org/10.1101/cshperspect.a016790); pmid: 24186068
- M. A. Stamnes, J. E. Rothman, The binding of AP-1 clathrin adaptor particles to Golgi membranes requires ADP-ribosylation factor, a small GTP-binding protein. *Cell* **73**, 999–1005 (1993). doi: [10.1016/0092-8674\(93\)90277-W](https://doi.org/10.1016/0092-8674(93)90277-W); pmid: 8500185
- L. M. Traub, J. A. Ostrom, S. Kornfeld, Biochemical dissection of AP-1 recruitment onto Golgi membranes. *J. Cell Biol.* **123**, 561–573 (1993). doi: [10.1083/jcb.123.3.561](https://doi.org/10.1083/jcb.123.3.561); pmid: 8227126
- L. P. Jackson *et al.*, A large-scale conformational change couples membrane recruitment to cargo binding in the AP2 clathrin adaptor complex. *Cell* **141**, 1220–1229 (2010). doi: [10.1016/j.cell.2010.05.006](https://doi.org/10.1016/j.cell.2010.05.006); pmid: 20603002
- B. J. Canagarajah, X. Ren, J. S. Bonifacino, J. H. Hurley, The clathrin adaptor complexes as a paradigm for membrane-associated allostery. *Protein Sci.* **22**, 517–529 (2013). doi: [10.1002/pro.2235](https://doi.org/10.1002/pro.2235); pmid: 23424177
- X. Ren, G. G. Fariás, B. J. Canagarajah, J. S. Bonifacino, J. H. Hurley, Structural basis for recruitment and activation of the AP-1 clathrin adaptor complex by Arf1. *Cell* **152**, 755–767 (2013). pmid: 23415225
- M. H. Malim, M. Emerman, HIV-1 accessory proteins—Ensuring viral survival in a hostile environment. *Cell Host Microbe* **3**, 388–398 (2008). doi: [10.1016/j.chom.2008.04.008](https://doi.org/10.1016/j.chom.2008.04.008); pmid: 18541215
- D. R. Collins, K. L. Collins, HIV-1 accessory proteins adapt cellular adaptors to facilitate immune evasion. *PLoS Pathog.* **10**, e1003851 (2014). doi: [10.1371/journal.ppat.1003851](https://doi.org/10.1371/journal.ppat.1003851); pmid: 24465204
- J. V. Garcia, A. D. Miller, Serine phosphorylation-independent downregulation of cell-surface CD4 by nef. *Nature* **350**, 508–511 (1991). pmid: 2014052
- C. Aiken, J. Konner, N. R. Landau, M. E. Lenburg, D. Trono, Nef induces CD4 endocytosis: Requirement for a critical dileucine motif in the membrane-proximal CD4 cytoplasmic domain. *Cell* **76**, 853–864 (1994). doi: [10.1016/0092-8674\(94\)90360-3](https://doi.org/10.1016/0092-8674(94)90360-3); pmid: 8124721
- O. Schwartz, V. Maréchal, S. Le Gall, F. Lemonnier, J.-M. Heard, Endocytosis of major histocompatibility complex class I molecules is induced by the HIV-1 Nef protein. *Nat. Med.* **2**, 338–342 (1996). doi: [10.1038/nm0396-338](https://doi.org/10.1038/nm0396-338); pmid: 8612235
- S. J. D. Neil, T. Zang, P. D. Bieniasz, Tetherin inhibits retrovirus release and is antagonized by HIV-1 Vpu. *Nature* **451**, 425–430 (2008). doi: [10.1038/nature06553](https://doi.org/10.1038/nature06553); pmid: 18200009
- J. F. Roeth, M. Williams, M. R. Kasper, T. M. Filzen, K. L. Collins, HIV-1 Nef disrupts MHC-I trafficking by recruiting AP-1 to the MHC-I cytoplasmic tail. *J. Cell Biol.* **167**, 903–913 (2004). doi: [10.1083/jcb.200407031](https://doi.org/10.1083/jcb.200407031); pmid: 15569716
- X. Jia *et al.*, Structural basis of HIV-1 Vpu-mediated BST2 antagonism via hijacking of the clathrin adaptor protein complex 1. *eLife* **3**, e02362 (2014). pmid: 24843023
- S. Le Gall *et al.*, Nef interacts with the mu subunit of clathrin adaptor complexes and reveals a cryptic sorting signal in MHC I molecules. *Immunity* **8**, 483–495 (1998). doi: [10.1016/S1074-7613\(00\)80553-1](https://doi.org/10.1016/S1074-7613(00)80553-1); pmid: 9586638
- R. Chaudhuri, O. W. Lindwasser, W. J. Smith, J. H. Hurley, J. S. Bonifacino, Downregulation of CD4 by human immunodeficiency virus type 1 Nef is dependent on clathrin and involves direct interaction of Nef with the AP2 clathrin adaptor. *J. Virol.* **81**, 3877–3890 (2007). doi: [10.1128/JVI.02725-06](https://doi.org/10.1128/JVI.02725-06); pmid: 17267500
- B. Doray, I. Lee, J. Knisely, G. Bu, S. Kornfeld, The γ/α 1 and α/α 2 hemicomplexes of clathrin adaptors AP-1 and AP-2 harbor the dileucine recognition site. *Mol. Biol. Cell* **18**, 1887–1896 (2007). doi: [10.1091/mbc.E07-01-0012](https://doi.org/10.1091/mbc.E07-01-0012); pmid: 17360967
- X. Jia *et al.*, Structural basis of evasion of cellular adaptive immunity by HIV-1 Nef. *Nat. Struct. Mol. Biol.* **19**, 701–706 (2012). doi: [10.1038/nsmb.2328](https://doi.org/10.1038/nsmb.2328); pmid: 22705789
- X. Ren, S. Y. Park, J. S. Bonifacino, J. H. Hurley, How HIV-1 Nef hijacks the AP-2 clathrin adaptor to downregulate CD4. *eLife* **3**, e01754 (2014). doi: [10.7554/eLife.01754](https://doi.org/10.7554/eLife.01754); pmid: 24473078
- K. Janvier *et al.*, HIV-1 Nef stabilizes the association of adaptor protein complexes with membranes. *J. Biol. Chem.* **278**, 8725–8732 (2003). doi: [10.1074/jbc.M210115200](https://doi.org/10.1074/jbc.M210115200); pmid: 12486136
- S. H. Coleman, D. Hitchin, C. M. Novello, J. C. Guatelli, HIV-1 Nef stabilizes AP-1 on membranes without inducing ARF1-independent de novo attachment. *Virology* **345**, 148–155 (2006). pmid: 16235302
- E. R. Wonderlich *et al.*, ADP ribosylation factor 1 activity is required to recruit AP-1 to the major histocompatibility complex class I (MHC-I) cytoplasmic tail and disrupt MHC-I trafficking in HIV-1-infected primary T cells. *J. Virol.* **85**, 12216–12226 (2011). doi: [10.1128/JVI.00056-11](https://doi.org/10.1128/JVI.00056-11); pmid: 21917951
- S. Jäger *et al.*, Global landscape of HIV-human protein complexes. *Nature* **481**, 365–370 (2012). pmid: 22190034
- Single-letter abbreviations for the amino acid residues are as follows: A, Ala; C, Cys; D, Asp; E, Glu; F, Phe; G, Gly; H, His; I, Ile; K, Lys; L, Leu; M, Met; N, Asn; P, Pro; Q, Gln; R, Arg; S, Ser; T, Thr; V, Val; W, Trp; and Y, Tyr.
- E. E. Heldwein *et al.*, Crystal structure of the clathrin adaptor protein 1 core. *Proc. Natl. Acad. Sci. U.S.A.* **101**, 14108–14113 (2004). doi: [10.1073/pnas.0406102101](https://doi.org/10.1073/pnas.0406102101); pmid: 15377783
- X. Yu, M. Breitman, J. Goldberg, A structure-based mechanism for Arf1-dependent recruitment of coatmer to membranes. *Cell* **148**, 530–542 (2012). doi: [10.1016/j.cell.2012.01.015](https://doi.org/10.1016/j.cell.2012.01.015); pmid: 22304919
- A. Fotin *et al.*, Molecular model for a complete clathrin lattice from electron cryomicroscopy. *Nature* **432**, 573–579 (2004). doi: [10.1038/nature03079](https://doi.org/10.1038/nature03079); pmid: 15502812
- J. Cherfils, Arf GTPases and their effectors: Assembling multivalent membrane-binding platforms. *Curr. Opin. Struct. Biol.* **29**, 67–76 (2014). doi: [10.1016/j.sbi.2014.09.007](https://doi.org/10.1016/j.sbi.2014.09.007); pmid: 25460270
- K. Janvier *et al.*, Recognition of dileucine-based sorting signals from HIV-1 Nef and LIMP-II by the AP-1 γ/α 1 and AP-3 δ/α 3 hemicomplexes. *J. Cell Biol.* **163**, 1281–1290 (2003). doi: [10.1083/jcb.200307157](https://doi.org/10.1083/jcb.200307157); pmid: 14691137
- N. L. Riggs, H. M. Craig, M. W. Pandori, J. C. Guatelli, The dileucine-based sorting motif in HIV-1 Nef is not required for down-regulation of class I MHC. *Virology* **258**, 203–207 (1999). doi: [10.1006/viro.1999.9736](https://doi.org/10.1006/viro.1999.9736); pmid: 10366557
- M. S. Robinson, J. S. Bonifacino, Adaptor-related proteins. *Curr. Opin. Cell Biol.* **13**, 444–453 (2001). doi: [10.1016/S0955-0674\(00\)00235-0](https://doi.org/10.1016/S0955-0674(00)00235-0); pmid: 11454451
- E. Cocucci, F. Aguet, S. Boulant, T. Kirchhausen, The first five seconds in the life of a clathrin-coated pit. *Cell* **150**, 495–507 (2012). doi: [10.1016/j.cell.2012.05.047](https://doi.org/10.1016/j.cell.2012.05.047); pmid: 22863004
- S. O. Dodonova *et al.*, A structure of the COPI coat and the role of coat proteins in membrane vesicle assembly. *Science* **349**, 195–198 (2015). doi: [10.1126/science.1254836](https://doi.org/10.1126/science.1254836); pmid: 26160949
- S. F. Kluge *et al.*, Nef proteins of epidemic HIV-1 group O strains antagonize human tetherin. *Cell Host Microbe* **16**, 639–650 (2014). doi: [10.1016/j.chom.2014.10.002](https://doi.org/10.1016/j.chom.2014.10.002); pmid: 25525794
- S. Watanabe *et al.*, Clathrin regenerates synaptic vesicles from endosomes. *Nature* **515**, 228–233 (2014). doi: [10.1038/nature13846](https://doi.org/10.1038/nature13846); pmid: 25296249
- B. T. Kelly *et al.*, AP2 controls clathrin polymerization via a membrane-activated switch. *Science* **345**, 459–463 (2014). doi: [10.1126/science.1254836](https://doi.org/10.1126/science.1254836); pmid: 25061211
- C. Suloway *et al.*, Automated molecular microscopy: The new Legion system. *J. Struct. Biol.* **151**, 41–60 (2005). doi: [10.1016/j.jsb.2005.03.010](https://doi.org/10.1016/j.jsb.2005.03.010); pmid: 15890530
- X. Li *et al.*, Electron counting and beam-induced motion correction enable near-atomic-resolution single-particle cryo-EM. *Nat. Methods* **10**, 584–590 (2013). doi: [10.1038/nmeth.2472](https://doi.org/10.1038/nmeth.2472); pmid: 23644547
- S. H. W. Scheres, R. Núñez-Ramírez, C. O. S. Sorzano, J. M. Carazo, R. Marabini, Image processing for electron microscopy single-particle analysis using XMIPP. *Nat. Protoc.* **3**, 977–990 (2008). doi: [10.1038/nprot.2008.62](https://doi.org/10.1038/nprot.2008.62); pmid: 18536645
- S. H. W. Scheres *et al.*, Maximum-likelihood multi-reference refinement for electron microscopy images. *J. Mol. Biol.* **348**, 139–149 (2005). doi: [10.1016/j.jmb.2005.02.031](https://doi.org/10.1016/j.jmb.2005.02.031); pmid: 15808859
- M. Radermacher, T. Wagenknecht, A. Verschoor, J. Frank, Three-dimensional reconstruction from a single-exposure, random conical tilt series applied to the 50S ribosomal subunit of *Escherichia coli*. *J. Microsc.* **146**, 113–136 (1987). doi: [10.1111/j.1365-2818.1987.tb01333.x](https://doi.org/10.1111/j.1365-2818.1987.tb01333.x); pmid: 3302267
- S. H. W. Scheres, RELION: Implementation of a Bayesian approach to cryo-EM structure determination. *J. Struct. Biol.* **180**, 519–530 (2012). doi: [10.1016/j.jsb.2012.09.006](https://doi.org/10.1016/j.jsb.2012.09.006); pmid: 23000701

46. N. R. Voss, C. K. Yoshioka, M. Radermacher, C. S. Potter, B. Carragher, DoG Picker and TiltPicker: Software tools to facilitate particle selection in single particle electron microscopy. *J. Struct. Biol.* **166**, 205–213 (2009). doi: [10.1016/j.jsb.2009.01.004](https://doi.org/10.1016/j.jsb.2009.01.004); pmid: [19374019](https://pubmed.ncbi.nlm.nih.gov/19374019/)
47. G. C. Lander *et al.*, Appion: An integrated, database-driven pipeline to facilitate EM image processing. *J. Struct. Biol.* **166**, 95–102 (2009). doi: [10.1016/j.jsb.2009.01.002](https://doi.org/10.1016/j.jsb.2009.01.002); pmid: [19263523](https://pubmed.ncbi.nlm.nih.gov/19263523/)
48. E. F. Pettersen *et al.*, UCSF Chimera—A visualization system for exploratory research and analysis. *J. Comput. Chem.* **25**, 1605–1612 (2004). doi: [10.1002/jcc.20084](https://doi.org/10.1002/jcc.20084); pmid: [15264254](https://pubmed.ncbi.nlm.nih.gov/15264254/)
49. T. Shiba *et al.*, Molecular mechanism of membrane recruitment of GGA by ARF in lysosomal protein transport. *Nat. Struct. Biol.* **10**, 386–393 (2003). doi: [10.1038/nsb920](https://doi.org/10.1038/nsb920); pmid: [12679809](https://pubmed.ncbi.nlm.nih.gov/12679809/)

ACKNOWLEDGMENTS

We thank E. Nogales for suggestions and advice; J. Bonifacino for discussions; P. Grob, S. Wu, Y. Cheng, and B. LaFrance for assistance at the outset of the project; and A. Johnson for assistance with figure preparation. This work was supported by the HARC Collaborative Opportunity Fund (J.H.H.; subaward of NIH grant P50GM082250 to A. Frankel) and NIH grant R01AI120691 (J.H.H.). EM facilities were supported by the Howard Hughes

Medical Institute (E. Nogales). All EM maps have been deposited in the Electron Microscopy Data Bank (accession codes: EMD-6385 for closed trimer, EMD-6388 for closed monomer, EMD-6389 for open trimer).

SUPPLEMENTARY MATERIALS

www.sciencemag.org/content/350/6259/aac5137/suppl/DC1
Figs. S1 to S10
Movies S1 and S2

5 May 2015; accepted 4 September 2015
[10.1126/science.aac5137](https://doi.org/10.1126/science.aac5137)



HIV-1 Nef hijacks clathrin coats by stabilizing AP-1:Arf1 polygons

Qing-Tao Shen *et al.*

Science **350**, (2015);

DOI: 10.1126/science.aac5137

This copy is for your personal, non-commercial use only.

If you wish to distribute this article to others, you can order high-quality copies for your colleagues, clients, or customers by [clicking here](#).

Permission to republish or repurpose articles or portions of articles can be obtained by following the guidelines [here](#).

The following resources related to this article are available online at www.sciencemag.org (this information is current as of February 22, 2016):

Updated information and services, including high-resolution figures, can be found in the online version of this article at:

</content/350/6259/aac5137.full.html>

Supporting Online Material can be found at:

</content/suppl/2015/10/21/350.6259.aac5137.DC1.html>

A list of selected additional articles on the Science Web sites **related to this article** can be found at:

</content/350/6259/aac5137.full.html#related>

This article **cites 48 articles**, 13 of which can be accessed free:

</content/350/6259/aac5137.full.html#ref-list-1>

This article appears in the following **subject collections**:

Biochemistry

</cgi/collection/biochem>